HARMONIC FUNCTIONS ON FINITELY-CONNECTED TORI

CHIU-YEN KAO, BRAXTON OSTING, AND ÉDOUARD OUDET

Abstract. In this paper, we prove a Logarithmic Conjugation Theorem on finitely-connected tori. The theorem states that a harmonic function can be written as the real part of a function whose derivative is analytic and a finite sum of terms involving the logarithm of the modulus of a modified Weierstrass sigma function. We implement the method using arbitrary precision and use the result to find approximate solutions to the Laplace problem and Steklov eigenvalue problem. Using a posteriori estimation, we show that the solution of the Laplace problem on a torus with a few holes has error less than 10^{-100} using a few hundred degrees of freedom and the Steklov eigenvalues have similar error.

BO: Revision due September 17, 2023.
BO: need to cite: [16].

1. Introduction

Harmonic functions satisfying the Laplace equation, $\Delta u = 0$, arise in many physical applications, including potential flow in fluid dynamics, the stationary solution of heat conduction, and electrostatics in the absence of charges, to name just a few. Efficient and robust numerical approaches to solving the Laplace equation on a general domain with different boundary conditions are crucial for understanding the aforementioned applications. In this paper, *we are particularly interested in solving the Laplace equation on finitely-connected tori*, which serves as a model problem for the study of heat or electrical conduction in the exterior of a periodic lattice of inclusions with prescribed temperature or for fluid flow through a doubly periodic array of obstacles.

Harmonic functions. It is well-known that every harmonic function u on a simply-connected domain $\Omega \subset \mathbb{C}$ can be written as the real part of an analytic function, $f(z)$,

$$u(z) = \Re f(z). \tag{1}$$

For finitely-connected domains, the analogous result is known as the *Logarithmic Conjugation Theorem* [2, 22]. Let $\Omega \subset \mathbb{C}$ be a finitely-connected region which means that $\mathbb{C} \setminus \Omega$ has only finitely many bounded connected components, $\{K_j\}_{j\in[b]}$ with $b \in \mathbb{N} \setminus \{0\}$. For each $j \in [b]$, let a_j be a point in K_j. If u is a harmonic function on Ω, then there exists an analytic function f on Ω and real numbers c_j, $j \in [b]$, such that

$$u(z) = \Re f(z) + \sum_{j\in[b]} c_j \log|z - a_j|, \qquad z \in \Omega. \tag{2}$$

Department of Mathematical Sciences, Claremont McKenna College, Claremont, CA
Department of Mathematics, University of Utah, Salt Lake City, UT
LJK, Université Grenoble Alpes, France
E-mail addresses: ckao@cmc.edu, osting@math.utah.edu, edouard.oudet@imag.fr.
Date: August 26, 2023.
2020 *Mathematics Subject Classification.* 30F15, 31A25, 35C10, 65N25.
Key words and phrases. Harmonic function; Laplace equation; finitely-connected torus; doubly-periodic domain; elliptic function; Weierstrass elliptic function; Steklov eigenvalue.

Our main result is to extend the Logarithmic Conjugation Theorem to finitely-connected tori. We consider a torus $\mathbb{T}_\omega = \mathbb{C}/L_\omega$, where $L_\omega = 2\omega_1\mathbb{Z} + 2\omega_2\mathbb{Z}$ is a lattice and $\omega = (\omega_1, \omega_2) \in \mathbb{C}^2$ are half-periods, assumed not to be colinear. Let

$$\Omega = \mathbb{T}_\omega \setminus \cup_{j\in[b]} K_j \tag{3}$$

denote the finitely-connected torus after removing $b \in \mathbb{N} \setminus \{0\}$ disjoint, connected compact sets $\{K_j\}_{j\in[b]}$, with smooth boundary. We also introduce the parallelogram (fundamental domain)

$$\mathcal{P} = \left\{2\omega_1 x + 2\omega_2 y \in \mathbb{C} \colon (x, y) \in [0, 1]^2\right\} \setminus \cup_{j\in[b]} K_j. \tag{4}$$

Note that Ω is obtained from $\mathcal{P}$ after identification of opposite sides. Recall that a meromorphic, doubly-periodic function is called an *elliptic* function. Let

$$\hat{\sigma}(z, \omega) = e^{-\frac{1}{2}\gamma_2 z^2 - \frac{1}{2}\pi|z|^2/A}\sigma(z, \omega) \tag{5}$$

denote the modified Weierstrass sigma function [14], where $\sigma(z, \omega)$ is the Weierstrass sigma function, $\gamma_2 = \gamma_2(\omega) \in \mathbb{C}$ is a lattice invariant, and $A = area(\mathbb{T}_\omega)$. We further discuss $\hat{\sigma}(z, \omega)$ in section 2, but for now just note that it is a non-holomorphic, function with a pole of order 2 at $z = 0$ such that $|\hat{\sigma}(z, \omega)|$ is doubly-periodic.

Theorem 1.1. *Let Ω and $\mathcal{P}$ be defined as in (3) and (4). For each $j \in [b]$, let a_j be a point in K_j. If u is a harmonic function on Ω (equivalently, harmonic and doubly-periodic on $\mathcal{P}$), then there exists an analytic function $\hat{f}$ on $\mathcal{P}$ and real numbers c_j, $j \in [b]$, satisfying $\sum_{j\in[b]} c_j = 0$, such that $\hat{f}'$ is elliptic and*

$$u(z) = \Re\hat{f}(z) + \sum_{j\in[b]} c_j \log|\hat{\sigma}(z - a_j, \omega)|, \qquad z \in \Omega. \tag{6}$$

If there is only one connected boundary component (i.e., $b = 1$), then $c_1 = 0$ and $u(z) = \Re\hat{f}(z)$.

A proof of theorem 1.1 is given in section 3. We comment that the result in theorem 1.1 differs from the Logarithmic Conjugation Theorem for finitely-connected domains in several important ways. First, the modified Weierstrass sigma function, $\log|\hat{\sigma}(z, \omega)|$, plays the role of $\log|z|$. Secondly, and perhaps surprisingly, while the derivative $\hat{f}'$ is elliptic, the function $\hat{f}$ cannot always be taken to be elliptic.

Computing harmonic functions on finitely-connected tori. There are a variety of methods for computing harmonic functions on finitely-connected tori, including integral equation methods with multipole acceleration [3] and the finite element method [13]. In our approach, we are inspired by the work in [22] to use theorem 1.1 to represent doubly-periodic harmonic functions using a series solution. Let $\wp(z) = \wp(z, \omega)$ denote the Weierstrass elliptic function, $\wp^{(k)}(z, \omega)$, denote the k-th derivative, and $\hat{\zeta}(z) = \hat{\zeta}(z, \omega)$ denote the "modified" form of the Weierstrass zeta function that is doubly-periodic; these will be defined in section 2.

Theorem 1.2. *Let Ω be a finitely-connected torus as in (3). For each $j \in [b]$, let a_j be a point in K_j. If u is a harmonic function on Ω, then there exists a constant $C \in \mathbb{R}$ and real coefficients $(a_{j,k})$, $(b_{j,k})$ and (c_j) such that*

$$\begin{aligned} u(z) = C + \sum_{j\in[b]} \Big[& a_{j,-1}\Re\hat{\zeta}(z - a_j) + b_{j,-1}\Im\hat{\zeta}(z - a_j) + \sum_{k\geq 0} a_{j,k}\Re\wp^{(k)}(z - a_j) + \sum_{k\geq 0} b_{j,k}\Im\wp^{(k)}(z - a_j) \\ & + c_j \log|\hat{\sigma}(z - a_j)| \Big] \end{aligned} \tag{7}$$

where $\sum_{j\in[b]} c_j = 0$.

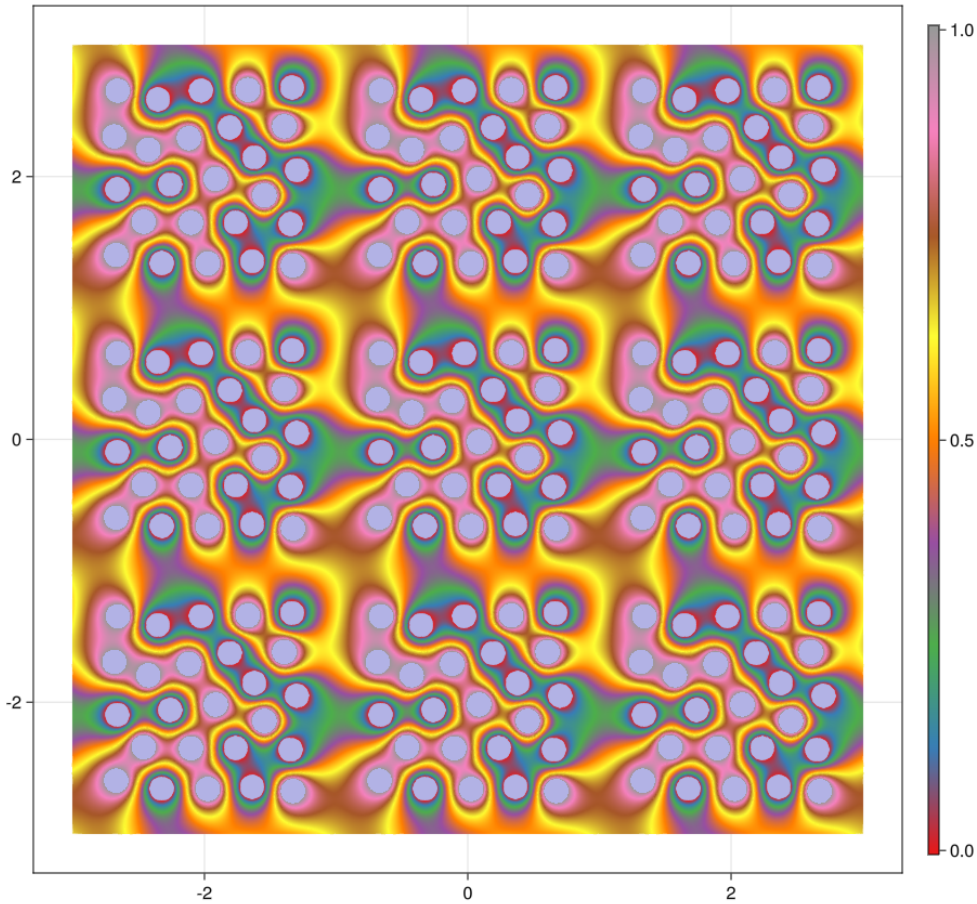

FIGURE 1. The solution of the Laplace equation on a square torus with 25 disks removed. Dirichlet boundary conditions equal to 0 or 1 are imposed on the boundary of each disk. The computational domain is $[-1,1]^2$ and 9 copies are displayed to emphasize periodicity. See section 4.2 for more details.

A proof of theorem 1.2 is given in section 3. We have chosen to represent the elliptic function f' using a sum of Weierstrass functions. Similar representations have been used to find doubly periodic solutions in several applications, including doubly-periodic stress distributions in perforated plates [17], solitary wave solutions to a nonlinear wave equation [8] and nonlinear Schrödinger equation [10], lowest-Landau-level wavefunctions on the torus [14], and simulation of oil recovery [1]. Other representations for elliptic functions are possible, including as $R(\wp) + \wp' S(\wp)$ for some rational functions R and S [7].

In section 4, we use the series representation (7) to solve the Laplace problem

$$\Delta u = 0 \quad \text{in } \Omega \tag{8a}$$

$$u = f \quad \text{on } \partial\Omega = \cup_{j\in[b]}\partial K_j, \tag{8b}$$

where $f \in L^2(\partial\Omega)$ is given and the Steklov eigenvalue problem

$$\Delta u = 0 \quad \text{in } \Omega \tag{9a}$$

$$\partial_n u = \sigma u \quad \text{on } \partial\Omega = \cup_{j\in[b]}\partial K_j. \tag{9b}$$

As in [22], the series solution (7) are not convergent series. The coefficients depend on the truncation of the sum (in k). For the Laplace problem, by the maximum principle, the accuracy of the solution can be computed by looking at the error on the boundary, $\sup_{x\in\partial\Omega}|u(x)-f(x)|$. For the Steklov problem, we bound the error in the eigenvalues using an a posteriori estimate [6, 11]. We implement the proposed numerical method in Julia using arbitrary precision and use the result to find approximate solutions to the Laplace problem and Steklov eigenvalue problem. For a few holes, the solution of the Laplace problem has error less than 10^{-100} using a few hundred degrees of freedom and the Steklov eigenvalues have similar error. We show the solution to the Laplace problem with 25 disks removed in fig. 1.

We conclude in section 5 with a discussion.

2. Weierstrass elliptic functions

Here we recall some background material on Weierstrass elliptic functions and establish notation used in the paper. Excellent references include [7, 14, 21].

We consider the lattice

$$L_\omega = 2\omega_1\mathbb{Z} + 2\omega_2\mathbb{Z},$$

where $\omega = (\omega_1, \omega_2) \in \mathbb{C}^2$ are half-periods, assumed not to be colinear. A function $f\colon \mathbb{C} \to \mathbb{C}$ is said to be *doubly-periodic* if it satisfies

$$f(z + 2\omega_1) = f(z)$$
$$f(z + 2\omega_2) = f(z)$$

for all $z \in \mathbb{C}$. A function is said to be *elliptic* if it is meromorphic and doubly-periodic. An example of an elliptic function is the Weierstrass elliptic function

$$\wp(z,\omega) := \frac{1}{z^2} + \sum_{\ell\in L_\omega\setminus\{0\}} \left(\frac{1}{(z-\ell)^2} - \frac{1}{(\ell)^2}\right).$$

The subtraction of the last term ensures the convergence of the series. Furthermore, the derivative of Weierstrass elliptic function is an odd function satisfying the differential equation

$$(\wp'(z))^2 = 4(\wp(z))^3 - g_2\wp(z) - g_3,$$

where $g_2 := \sum_{\ell\neq 0} 60\frac{1}{(\ell)^4}$ and $g_3 := \sum_{\ell\neq 0} 140\frac{1}{(\ell)^6}$. This differential equation can be used to compute higher-order derivatives of $\wp$. We obtain

$$\wp^{(2)}(z) = 6\wp^2(z) - \frac{g_2}{2}$$

and

$$\wp^{(n+2)}(z) = 6\sum_{k=0}^{n}\binom{n}{k}\wp^{(n-k)}(z)\wp^{(k)}(z), \qquad n \geq 1.$$

The Weierstrass zeta function is defined by

$$\zeta(z) = \frac{1}{z} + \sum_{\ell\neq 0}\left\{\frac{1}{z-\ell} + \frac{1}{\ell} + \frac{z}{\ell^2}\right\} = \frac{1}{z} + \sum_{\ell\neq 0}\frac{z^3}{\ell^2(z^2-\ell^2)} \tag{10}$$

and satisfies

$$\frac{d\zeta}{dz} = -\wp(z).$$

It has a Laurent expansion near $z = 0$

$$\zeta(z) = \frac{1}{z} - \sum_{k=2}^{\infty}\gamma_{2k}z^{2k-1},$$

where $\gamma_{2k} = \sum_{\ell \neq 0} \frac{1}{\ell^{2k}}$, $k \geq 2$. In contrast to $\wp(z)$, the function $\zeta(z)$ does not possess the double-periodic property. Instead, it satisfies the quasi-periodic condition:

$$\zeta(z + 2\omega_1) = \zeta(z) + 2\eta_1$$
$$\zeta(z + 2\omega_2) = \zeta(z) + 2\eta_2$$

where $\eta_1 = \zeta(\omega_1)$ and $\eta_2 = \zeta(\omega_2)$. The values η_1, η_2, ω_1, ω_2 are not independent but related by the Legendre identity

$$\eta_1\omega_2 - \eta_2\omega_1 = \frac{\pi\imath}{2}.$$

The ζ function can be modified so that it is periodic,

$$\hat{\zeta}(z) = \zeta(z) - \gamma_2 z - \frac{\pi}{A} z^*$$

where A is the area of the fundamental cell of the lattice and γ_2 is given by a Eisenstein summation and satisfies $\zeta(\omega_i) \equiv \eta_i = \gamma_2\omega_i + \frac{\pi\omega_i^*}{A}$, $i = 1, 2$ [14]. Note that since $\hat{\zeta}$ depends on z^*, it is no longer meromorphic.

Finally, the Weierstrass sigma function is defined by

$$\sigma(z, \omega) = \lim_{\varepsilon \to 0} \varepsilon \exp\left(\int_{\varepsilon}^{z} \zeta(w, \omega) dw\right),$$

which is an odd, non-doubly-periodic, holomorphic function function with simple zeros at the lattice points. It satisfies

$$\zeta(z, \omega) = \frac{\sigma'(z, \omega)}{\sigma(z, \omega)}. \tag{11}$$

As for the zeta function, the sigma function can be modified as in (5). When defined this way, its modulus has the lattice periodicity [14].

3. Proof of Theorems 1.1 and 1.2

Proof of theorem 1.1. The first part of the proof closely follows the proof of S. Axler for the Logarithmic Conjugation Theorem [2]. Define $h\colon \Omega \to \mathbb{C}$ by

$$h(z) := u_x(z) - \imath u_y(z).$$

The Cauchy-Riemann equations can be used to check that h is analytic on Ω. For each $j \in [b]$, let Γ_j be a closed curve in Ω that circles K_j once and no other K_k, $k \neq j$. Define

$$c_j := \frac{1}{2\pi\imath} \oint_{\Gamma_j} h(w)\ dw.$$

We see that $\Im c_j = -\frac{1}{2\pi}\Re \oint_{\Gamma_j} h(w)\ dw = -\frac{1}{2\pi}\Re \oint_{\Gamma_j} u_x(w)dx + u_y(w)dy = 0$, so c_j is a real number for each $j \in [b]$. Since u is doubly-periodic, so is h, and by the Cauchy Integral Theorem [9, Thm.1], we have that

$$\sum_{j \in [b]} c_j = 0. \tag{12}$$

We consider h to be a function on $\mathcal{P}$, which we still denote by h. Fix a point $z_0 \in \mathcal{P}$, and define $f\colon \mathcal{P} \to \mathbb{C}$ by

$$f(z) := \int_{z_0}^{z} h(w) - \sum_{j \in [b]} c_j \zeta(w - a_j, \omega)\ dw,$$

where the integral is taken over any path in $\mathcal{P}$ from z_0 to z and ζ is the Weierstrass zeta function as in (10). To show that f is well-defined, we check that the above integral is independent of the

path from z_0 to z. Take two paths from z_0 to z and reverse the direction of transversal in one to form a closed curve. Thus, we need only show that

$$\frac{1}{2\pi\imath}\oint_\gamma h(z)dw = \frac{1}{2\pi\imath}\sum_{j\in[b]} c_j \oint_\gamma \zeta(w-a_j,\omega)\ dw$$

for any closed curve γ Ω. By the Cauchy Integral Theorem and the definition of c_j, the left hand side is given by $\sum_{j\in[b]} c_j I_j(\gamma)$, where $I_j(\gamma)$ denotes the winding number of γ about K_j. Using that the Laurent expansion for $\zeta(z,\omega)$, which has a single pole of order one, by the Cauchy Integral Theorem, the right hand side is also seen to be equal to $\sum_{j\in[b]} c_j I_j(\gamma)$, as desired. The function $f(z)$ is analytic on $\mathcal{P}$ and we compute the derivative

$$f'(z) = h(z) - \sum_{j\in[b]} c_j\zeta(z-a_j,\omega). \tag{13}$$

Now define

$$q(z) := \Re f(z) + \sum_{j\in[b]} c_j \log|\sigma(z-a_j,\omega)|. \tag{14}$$

We claim that $u_x(z) = q_x(z)$ and $u_y(z) = q_y(z)$, so that, after adding a constant to f, we obtain $u(z) = q(z)$, $z\in\mathcal{P}$. Using (11), we compute

$$q_x(z) = \Re f'(z) + \sum_{j\in[b]} c_j\Re\zeta(z-a_j,\omega) = \Re h(z) = u_x.$$

and

$$q_y(z) = \Re\left(\imath f'(z)\right) + \sum_{j\in[b]} c_j\Re\left(\imath\zeta(z-a_j,\omega)\right) = \Re\left(\imath h(z)\right) = u_y.$$

We have established that $u(z) = q(z)$ up to a constant, $z\in\mathcal{P}$ and it remains to show that we can rewrite $q(z)$ in (14) so that the two terms on the right hand side are each doubly-periodic, so can be thought of as functions on Ω. In (14), the second term on the right hand side is not doubly-periodic since σ is not doubly-periodic. By (5), this term can be rewritten

$$\sum_{j\in[b]} c_j \log|\sigma(z-a_j)| = \sum_{j\in[b]} c_j \log|\hat{\sigma}(z-a_j)| + \Re g(z)$$

where

$$\begin{aligned} g(z) &= \frac{1}{2}\sum_{j\in[b]} c_j\left(\gamma_2(z-a_j)^2 + \pi|z-a_j|^2/A\right) \\ &= \alpha z + \beta z^* + \gamma, \end{aligned}$$

where α, β, and γ are constants and we have used (12) to drop the quadratic terms.

From (13), f' is doubly-periodic since h is doubly-periodic and $\sum_{j\in[b]} c_j = 0$. There exists α_1,α_2 such that for all admissible z

$$\begin{cases} f(z+2\omega_1) = f(z) + \alpha_1 \\ f(z+2\omega_2) = f(z) + \alpha_2. \end{cases}$$

Let us introduce (μ_1,μ_2) the unique solution of

$$\begin{cases} \omega_1\mu_1 + \omega_1^*\mu_2 = -\alpha_1/2. \\ \omega_2\mu_1 + \omega_2^*\mu_2 = -\alpha_2/2. \end{cases}$$

Notice that previous system is non singular since the determinant is proportional to the area of the fundamental domain, which is nonzero. Moreover, a straightforward computation shows that

$$f(z) + \mu_1 z + \mu_2 z^*$$

is a doubly-periodic function. Thus, for a suitable μ, $\hat{f}(z) = f(z) + \mu z$, is an analytic function and $\Re\hat{f}(z)$ is also doubly-periodic. Note that $\Im\hat{f}(z)$ is not necessarily doubly-periodic and $\hat{f}'$ is elliptic.

Summarizing our results, we have established that there exists $\hat{f}$ analytic with doubly-periodic real part and $(\nu, \xi) \in \mathbb{C}^2$ such that

$$u = \Re\hat{f} + \sum_{j\in[b]} c_j \log|\hat{\sigma}(z - a_j)| + \Re(\nu z + \xi z^*)$$

Observing that both the left hand side and the two first terms of the right hand side are doubly-periodic, we obtain $\nu = \xi = 0$, which concludes the proof. □

Proof of theorem 1.2. Let $\hat{f}'$ be the elliptic function from theorem 1.1 associated with the harmonic function u. Using a representation of elliptic functions (see, e.g., [23, p.450] or [21, p.23]), we may write

$$\hat{f}'(z) = \tau + \sum_{j\in[b]} \left(\alpha_j \zeta(z - a_j) + \sum_{k\geq 0} \beta_{j,k} \wp^{(k)}(z - a_j) \right),$$

where $\tau \in \mathbb{C}$, $\alpha_j \in \mathbb{C}$, and $\beta_{j,k} \in \mathbb{C}$ are constants. Consequently, there exists a constant $\rho \in \mathbb{C}$ such that

$$\hat{f}(z) = \tau z + \rho + \sum_{j\in[b]} \left(\alpha_j \log\sigma(z - a_j) + \beta_{j,0}\zeta(z - a_j) + \sum_{k\geq 1} \beta_{j,k} \wp^{(k-1)}(z - a_j) \right).$$

Introducing the periodic modifications $\hat{\zeta}$ and $\log|\hat{\sigma}|$ of ζ and $\log|\sigma|$ functions respectively, we obtain that there exists real coefficients $C, a_{j,k}, b_{j,k}$ such that

$$u(z) = C + \sum_{j\in[b]} \Big[a_{j,-1}\Re\hat{\zeta}(z - a_j) + b_{j,-1}\Im\hat{\zeta}(z - a_j) + \sum_{k\geq 0} a_{j,k}\Re\wp^{(k)}(z - a_j) + \sum_{k\geq 0} b_{j,k}\Im\wp^{(k)}(z - a_j) + c_j \log|\hat{\sigma}(z - a_j)| \Big] + g(x, y)$$

for some affine function g. By periodicity of all other terms, the function g has also to be doubly-periodic, so must be identically equal to zero. Finally, $\sum_{j\in[b]} c_j = 0$ is deduced from the harmonicity of all the terms, except the $\log|\hat{\sigma}|$ terms which have a constant Laplacian. □

4. Computational method and experiments

Here we develop a computational method based on a series solution of the form (7) to solve the Laplace problem (8) and the Steklov eigenvalue problem (9).

4.1. **Computational Method.** Let Ω be a finitely-connected torus as in (3). For simplicity, we will take each region K_j, $j \in [b]$ to be a closed disk, $K_j = \overline{B}(a_j, r_j)$, that is centered at the point a_j and has radius r_j. The centers and radii are chosen such that $K_i \cap K_j = \varnothing$ for $i \neq j$. Based on theorem 1.2, we consider a series solution of the form (7), where the sums on k are truncated at $k = k_{\max}$. We collect the (real) coefficients in the series solution into a vector $v = [C, (a_{j,k}), (b_{j,k}), (c_j)] \in \mathbb{R}^m$, where $m = 1 + 2b(k_{\max} + 2) + (b - 1)$. For each coefficeint, v_i, we let ϕ_i, $i \in [m]$ denote the corresponding basis function (e.g., the real part of a Weierstrass $\wp$ function), so that

$$u(z) = \sum_{i\in[m]} v_i \phi_i(z). \tag{15}$$

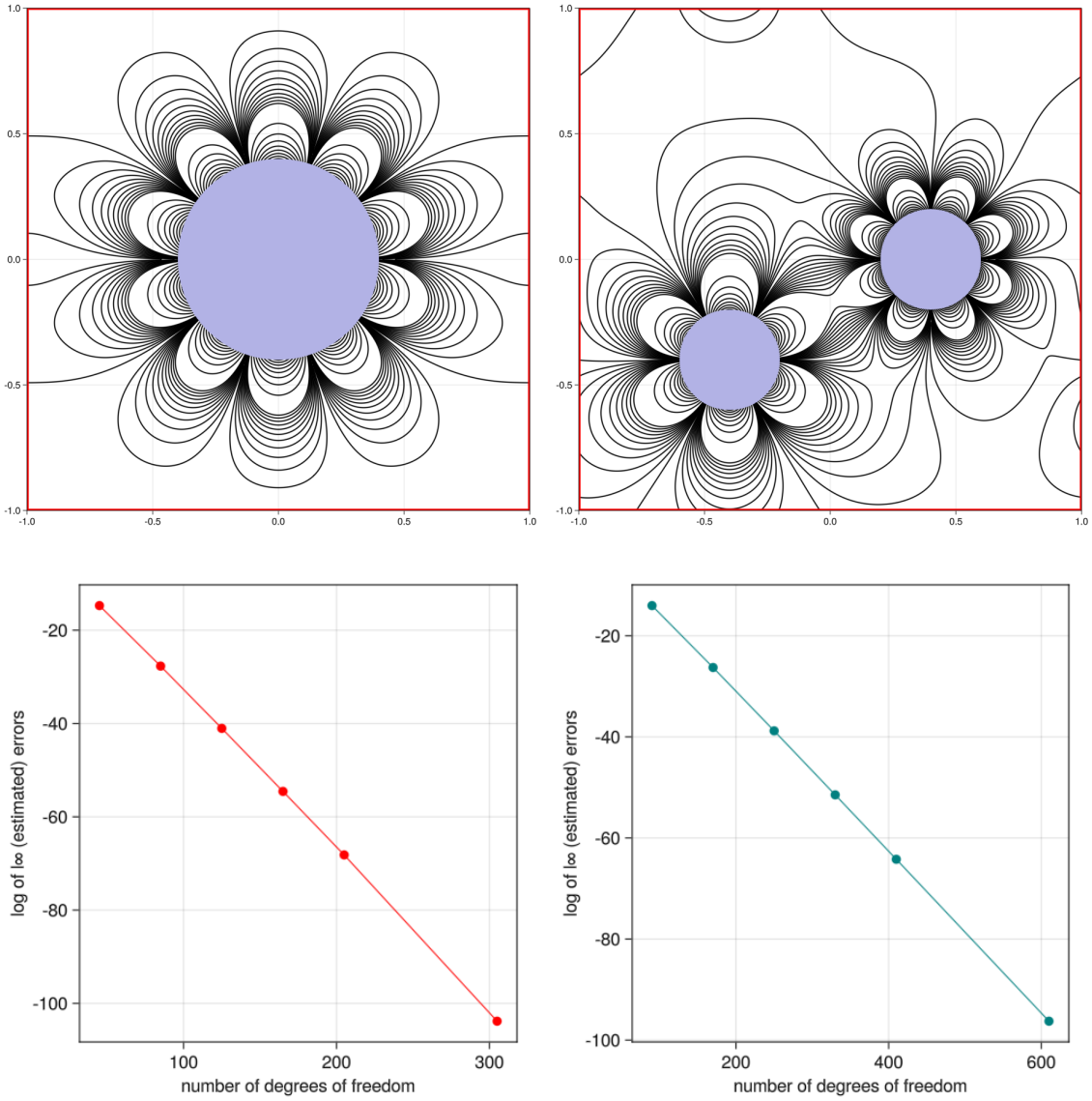

FIGURE 2. **(upper panels)** Approximation of the solutions of Laplace problem in a square torus with one and two holes. **(lower panels)** Spectral convergence for each of the two geometries. See section 4.2.

On each boundary component ∂K_j, we uniformly sample points with respect to arclength and denote the collection of all sampled points by $(p_\ell)_{\ell \in [S]}$. In the experiments below, we report the value of m and take $S = 3m$. Define the matrices $A, B \in \mathbb{R}^{S \times m}$ by

$$A_{\ell,i} = \frac{\partial \phi_i}{\partial n}(p_l)$$
$$B_{\ell,i} = \phi_i(p_l).$$

Details about the computation of the normal derivatives of basis functions are given in appendix A.

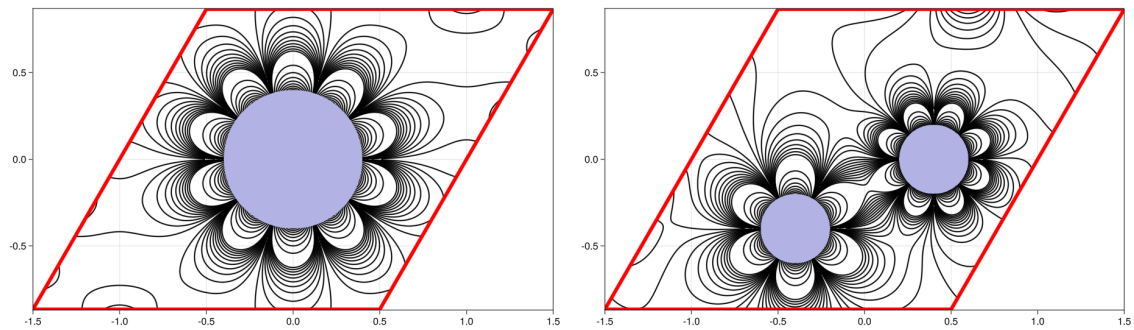

FIGURE 3. Approximation of the solutions of Laplace problem in an equilateral torus. See section 4.2.

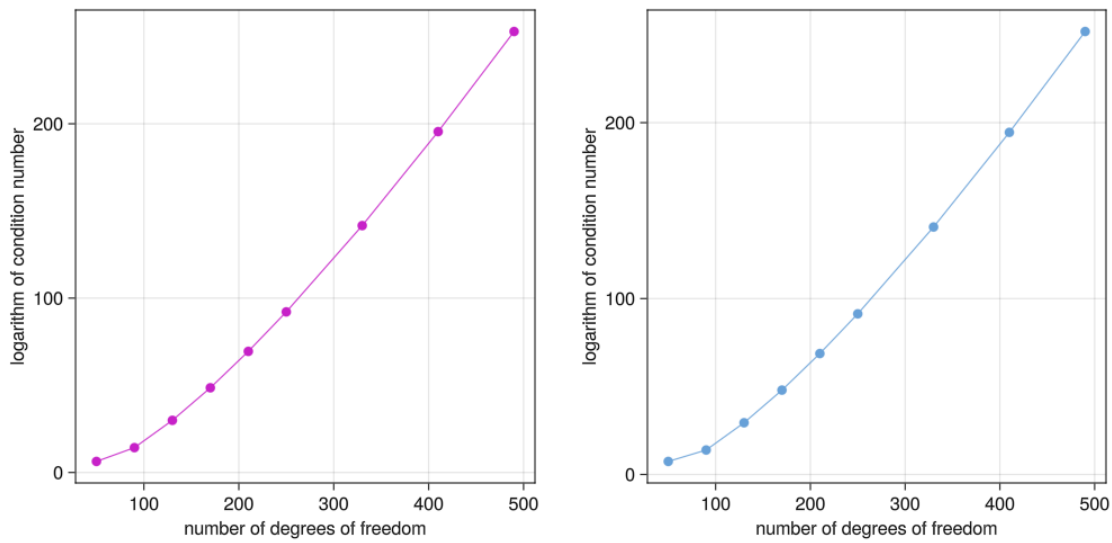

FIGURE 4. Exponential growth of conditional numbers of matrices B^tB (left) and B^tA (right) with respect to the number of degrees of freedom.

4.2. **Laplace problem.** We solve the Laplace problem (8), with boundary data $f(x)$, $x \in \partial\Omega$ as follows. Define the vector $b \in \mathbb{R}^S$ by $b_\ell = f(p_\ell)$. The least-squares solution is found by solving the normal equations

$$B^tBv = B^tb. \tag{16}$$

The solution v then is used with the expansion in (15) as an approximate solution of (8). By the maximum principle, the accuracy of the solution can be computed by looking at the error on the boundary, $\sup_{x\in\partial\Omega} |u(x) - f(x)|$.

We implement the numerical method in Julia using arbitrary precision provided by the packages *GenericLinearAlgebra.jl* and *ArbNumerics.jl* (a wrapper of the *Arb* C library). All computational experiments were performed with a precison of 2^{10} bits which corresponds to a machine epsilon approximately equal to 10^{-300}.

We first consider a finitely-connected square torus with half-periods $(\omega_1, \omega_2) = (1, i)$. The complement is taken to be $b = 1$ disks with $K_1 = B(a_1, r)$ with $a_1 = 0$ and $r = 0.4$. We take $f(\theta) = \sin(5\theta)$, where θ is the polar angle centered at a_1. The resulting solution is plotted in the

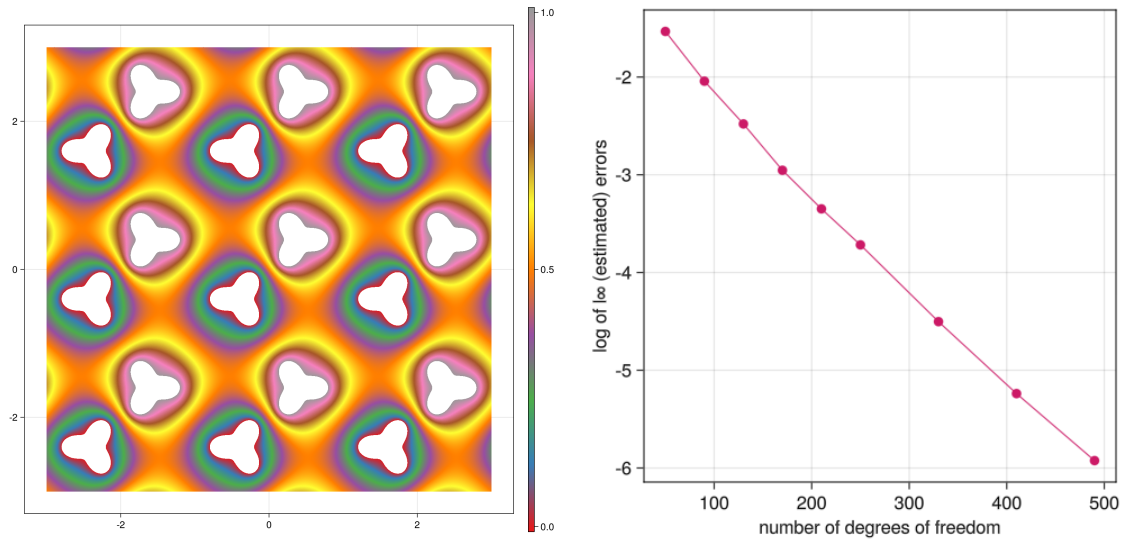

FIGURE 5. Approximation of the solutions of Laplace problem in a square torus with two non convex holes.

top left panel of fig. 2. Using the maximum principle to bound the $L^\infty(\Omega)$ error of the solution, we estimate $\|u(x) - f(x)\|_{L^\infty(\partial\Omega)}$ in the bottom left panel of fig. 2 for increasing number of degrees of freedom, m. This estimate is based on the maximum value obtained at the sampled points, after doubling the number of sampled points. Spectral convergence is observed. With $k_{\max} = 150$ ($m = 305$ degrees of freedom), the solution has error less 10^{-100} corresponding to at least 100 digits of accuracy.

Next, we again consider a finitely-connected square torus with half-periods $(\omega_1, \omega_2) = (1, i)$. The complement is taken to be $b = 2$ disks with $K_i = B(a_i, r_i)$, $i = 1, 2$ with $a_1 = 0.4$, $a_2 = -0.4 - 0.4i$ and $r_1 = r_2 = 0.2$. On each boundary, we set $f(\theta) = \sin(4\theta)$ for circle $i = 1$ and $f(\theta) = \sin(3\theta)$ for circle $i = 2$. The resulting solution is plotted in the top right panel of fig. 2. In the bottom right panel of fig. 2, we can see that the solutions have similar error as the previous example, albeit using more degrees of freedom.

Next, we consider a finitely-connected equilateral torus with half-periods $(\omega_1, \omega_2) = \left(1, \frac{1}{2} + \frac{\sqrt{3}}{2}\imath\right)$. The complement is taken to be the same sets as above with one and two holes. We plot the results in fig. 3. The solutions have similar error to the previous examples.

In fig. 5, we provide an example of convergence of the Laplace problem for two non-convex holes in a square torus. The polar parametrizations of the boundaries of the two holes K_1 and K_2 are given by $\rho(\theta)(\cos(\theta), \sin(\theta)) + A_i$ where

$$\rho(\theta) = \frac{3}{10} + \frac{\cos(3\theta)}{10}$$

and $A_1 = (0.4, 0.4)$ and $A_2 = -A_1$. The second hole has been rotated clockwise by an angle of $\frac{\pi}{3}$. We impose the Dirichlet condition 0 on the first boundary component and 1 on the second. The sampled points are obtained using previous parametrization together with a uniform samplings of the angles. As previously, we observe the exponential convergence and notice that the obtained accuracy is significantly lower than in previous cases with the same number of degrees of freedom.

Finally, we consider the Laplace equation on a finitely-connected square torus with 25 disks removed. Dirichlet boundary conditions equal to 0 or 1 are imposed on the boundary of each disk. The results are plotted in fig. 1. The solution has error less than 10^{-16}.

4.3. **Steklov eigenvalue problem.** To solve the Steklov eigenvalue problem (9), we consider a generalized eigenvalue problem

$$A\ v = \sigma B\ v. \tag{17}$$

We can approximate solutions to this eigenvalue problem by multiplying both sides by B^t and considering the non-symmetric generalized eigenvalue problem, $B^t A v = \sigma B^t B v$. For $k_{max} \leq 50$, this formulation leads to exponentially converging eigenvalue approximations, as expected. As it has been observed by several authors [5, 4, 11], this formulation with a larger number of degrees of freedom may produce ill-conditioned matrices. To overcome this difficulty and avoid spurious modes, we followed the SVD approach described in [5]: For a (small) set of randomly sampled interior points $(q_r)_{r\in[R]}$ we consider the evaluation matrix $C \in \mathbb{R}^{R\times m}$

$$C_{r,i} = \phi_i(q_r) \tag{18}$$

In all our experiments we set $R = 50$. We define $s(\sigma)$ to be the smallest (always non-negative) eigenvalue of the generalized eigenvalue problem

$$D(\sigma)x(\sigma) = s(\sigma)C^t C x(\sigma) \tag{19}$$

where $D(\sigma) = (A - \sigma B)^t (A - \sigma B)$. From a computational point of view, $s(\sigma)$ can be efficiently evaluated using a standard power method or an orthogonal subspace approach if the multiplicity is suspected to be greater than one. Local minimizers of $s(\sigma)$ provide stable approximations of Steklov eigenvalues. To identify numerically these local extrema, we used a classical golden section algorithm.

To bound the error in the eigenvalues, we use the following a posteriori estimate for Steklov eigenvalues in [6], which extends previous estimates for Laplace-Dirichlet eigenvalues [11, 19].

Proposition 4.1 ([6])**.** *Consider Ω a bounded open regular domain, and suppose that u_ε solve the following approximate eigenvalue problem*

$$\begin{aligned} -\Delta u_\varepsilon &= 0 && \text{in } \Omega \\ \partial_n u_\varepsilon &= \sigma_\varepsilon u_\varepsilon + f_\varepsilon && \text{on } \partial\Omega. \end{aligned}$$

Then if $\|f_\varepsilon\|_{L^2(\partial\Omega)}$ is small, there exists a constant C, depending only on Ω, and a Steklov eigenvalue σ_k satisfying

$$\frac{|\sigma_\varepsilon - \sigma_k|}{\sigma_k} \leq C\|f_\varepsilon\|_{L^2(\partial\Omega)}.$$

We study three geometrical configurations: tori which are the complement of $K_1 = B(a_1, r)$ with $a_1 = 0$ and $r = 0.4$, the complement of $K_i = B(a_i, r_i)$, $i = 1, 2$ with $a_1 = 0.2$, $a_2 = -0.2 + 0.2i$ and $r_1 = r_2 = 0.1$ and the complement of $K_i = B(a_i, r_i)$, $i = 1, 2, 3$ with $a_1 = 0.3$, $a_2 = 0.3i$, $a_3 = -0.3 - 0.3i$ and $r_1 = r_2 = 0.1$, $r_3 = 0.05$. We approximated Steklov eigenfunctions of the square torus with half-periods $(\omega_1, \omega_2) = (1, i)$ (see figs. 6 to 8) and of the equilateral torus with half-periods $(\omega_1, \omega_2) = \left(1, \frac{1}{2} + \frac{\sqrt{3}}{2}\imath\right)$ in these three configurations (see figs. 9 to 11). The first eigenvalue is zero which corresponds to a constant eigenfunction. In these figures, Steklov eigenfunctions of indices 2 to 7 are plotted. The Steklov eigenfunctions, as expected, are oscillatory near the boundary and decay exponentially away from the boundary. We used proposition 4.1 to estimate the approximation error of the Steklov eigenvalues. We approximated the L^2 boundary term by a (periodic) trapezoidal quadrature formula after doubling the number of sampled points. Convergence plots for Steklov eigenvalues on a square domain with 1, 2, and 3 punctured holes are given in fig. 12. As expected, spectral convergence is also observed in these situations. The same convergence rate has also been obtained studying the equilateral case.

Finally, in appendix B, we report in tables 1 to 6 our approximation of the first six non-trivial eigenvalues of the square and equilateral tori with $b = 1$, 2, and 3 holes. We believe that the reported

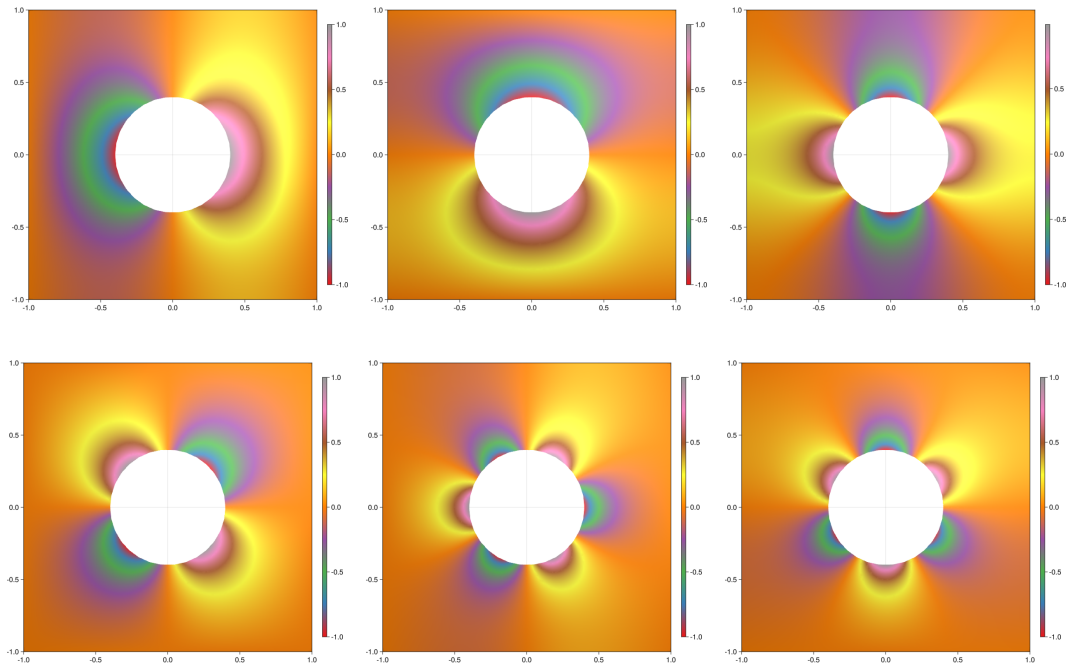

FIGURE 6. Steklov eigenfunctions of indices 2 to 7 of a punctured square torus, with one hole. See section 4.3.

50 digits are correct in each case. As indicated in theorem 1.1, when there is only one connected boundary component ($b = 1$), the eigenfunctions do not involve the logarithmic term and are oscillatory along the boundary as shown in figs. 6 and 9. In general, eigenfunctions corresponding to larger Steklov eigenvalues are more oscillatory near the boundary. Note that the tori parameters, ω, effects the multiplicity of the eigenvalues. On a square torus with one hole, $\sigma_2 = \sigma_3$ and $\sigma_6 = \sigma_7$ while, on an equilateral torus with one hole, $\sigma_2 = \sigma_3$ and $\sigma_4 = \sigma_5$. Since the domains with two or three holes do not possess symmetry, we observe that all the obtained eigenvalues are simple.

5. Discussion

In this paper, we established theorem 1.1, a Logarithmic Conjugation Theorem on finitely-connected tori. We used the theorem to find a series solution representation of harmonic functions on finitely-connected tori; see theorem 1.2. Implementing the numerical method in Julia using arbitrary precision, we approximate solutions to the Laplace problem (8) and the Steklov eigenvalue problem (9); see section 4. Using a posteriori estimation, we show that the approximate solution of the Laplace problem has error less than 10^{-100} using a few hundred degrees of freedom and the Steklov eigenvalues have similar error.

There are several future directions for this work. In [18], it is shown that the fundamental solution of Laplacian on flat tori can be expressed as a logarithmic function involving first Jacobi theta function; we think it would be interesting to extend this to finitely-connected tori. We have focused on the case where the domain complement, $\cup_{j\in[b]} K_j$ has smooth boundary. We think it would be interesting to extend the methods in [12] to improve the order of convergence for non-smooth boundaries. Finally, we think it would be interesting to apply the developed numerical methods to the numerical problem of computing extremal Steklov eigenvalue problems for finitely-connected flat tori [15, 20].

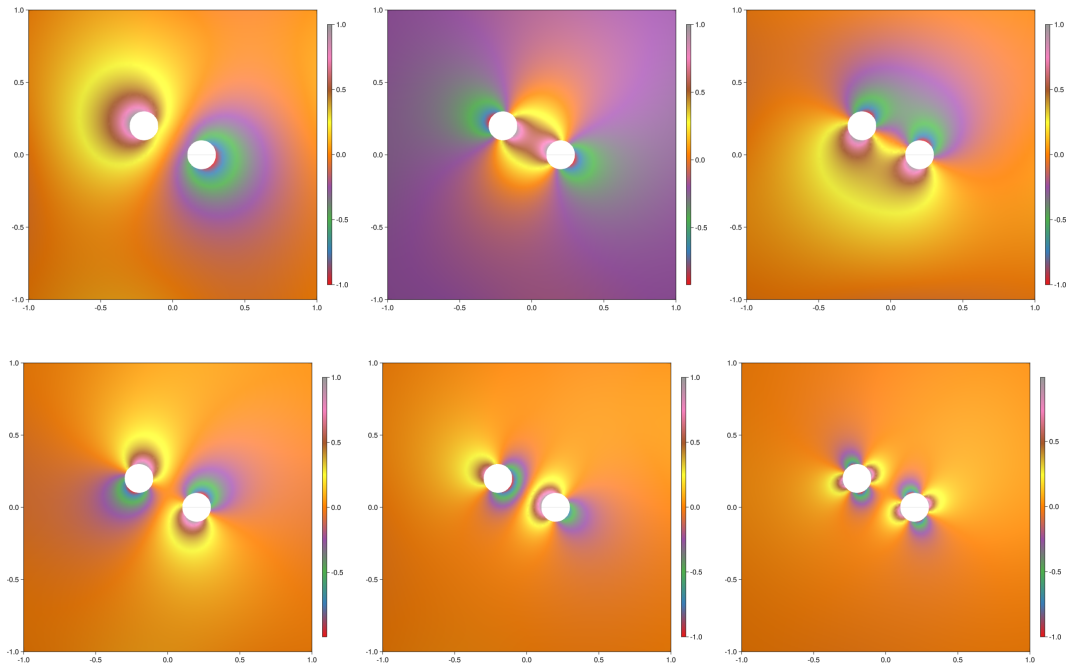

FIGURE 7. Steklov eigenfunctions of indices 2 to 7 of a punctured square torus, with two holes. See section 4.3.

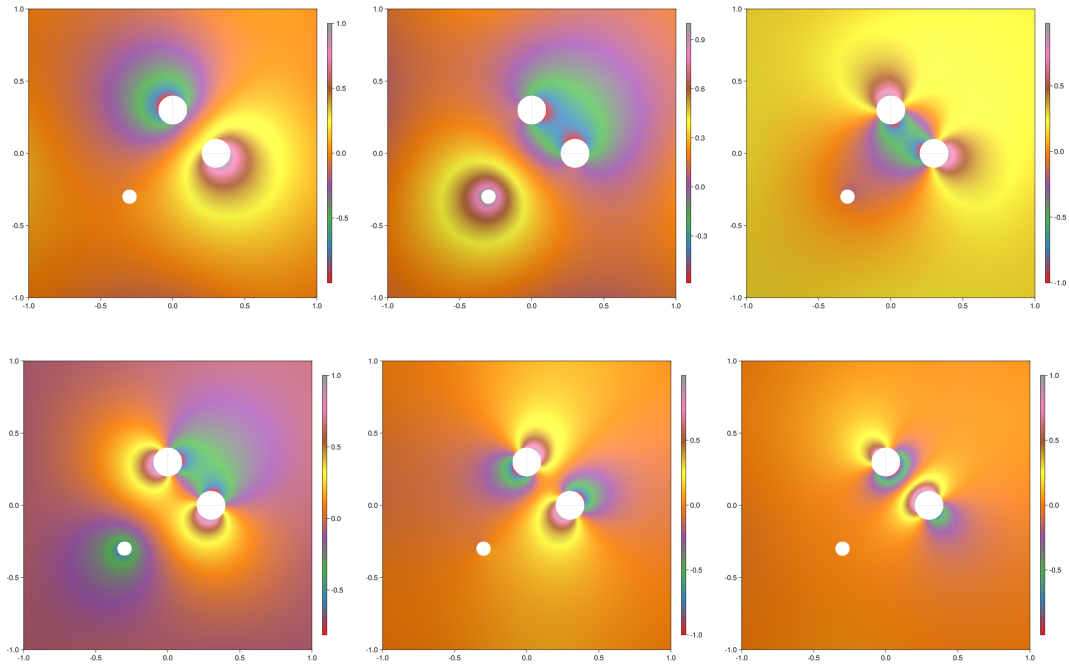

FIGURE 8. Steklov eigenfunctions of indices 2 to 7 of a punctured square torus, with three holes. See section 4.3.

References

[1] V. I. Astafev and P. V. Roters, *Simulation of oil recovery using the Weierstrass elliptic functions*, International Journal of Mechanics, 8 (2014), pp. 359–370.

[2] S. Axler, *Harmonic functions from a complex analysis viewpoint*, The American Mathematical Monthly, 93 (1986), p. 246.

[3] A. H. Barnett, G. R. Marple, S. Veerapaneni, and L. Zhao, *A unified integral equation scheme for doubly periodic Laplace and Stokes boundary value problems in two dimensions*, Communications on Pure and Applied Mathematics, 71 (2018), pp. 2334–2380.

[4] T. Betcke, *The generalized singular value decomposition and the method of particular solutions*, SIAM Journal on Scientific Computing, 30 (2008), pp. 1278–1295.

[5] T. Betcke and L. N. Trefethen, *Reviving the method of particular solutions*, SIAM Review, 47 (2005), pp. 469–491.

[6] B. Bogosel, *The method of fundamental solutions applied to boundary eigenvalue problems*, Journal of Computational and Applied Mathematics, 306 (2016), pp. 265–285.

[7] R. Busam and E. Freitag, *Complex Analysis*, 2009.

[8] Y. Chen and Z. Yan, *The Weierstrass elliptic function expansion method and its applications in nonlinear wave equations*, Chaos, Solitons & Fractals, 29 (2006), pp. 948–964.

[9] V. V. Datar, *Lecture notes on generalized Cauchy's theorem*, 2016.

[10] A. El Achab, *Constructing of exact solutions to the nonlinear Schrödinger equation (nlse) with power-law nonlinearity by the Weierstrass elliptic function method*, Optik, 127 (2016), pp. 1229–1232.

[11] L. Fox, P. Henrici, and C. Moler, *Approximations and bounds for eigenvalues of elliptic operators*, SIAM Journal on Numerical Analysis, 4 (1967), pp. 89–102.

[12] A. Gopal and L. N. Trefethen, *Solving Laplace problems with corner singularities via rational functions*, SIAM Journal on Numerical Analysis, 57 (2019), pp. 2074–2094.

[13] J. M. Guedes and N. Kikuchi, *Preprocessing and postprocessing for materials based on the homogenization method with adaptive finite element methods*, Computer methods in applied mechanics and engineering, 83 (1990), pp. 143–198.

[14] F. D. M. Haldane, *A modular-invariant modified Weierstrass sigma-function as a building block for lowest-Landau-level wavefunctions on the torus*, Journal of Mathematical Physics, 59 (2018), p. 071901.

[15] C.-Y. Kao, B. Osting, and E. Oudet, *Computational approaches for extremal geometric eigenvalue problems*, in Handbook of Numerical Analysis, Elsevier, 2022.

[16] C.-S. Lin and C.-L. Wang, *Elliptic functions, green functions and the mean field equations on tori*, Annals of Mathematics, 172 (2010), pp. 911–954.

[17] A. M. Linkov and V. F. Koshelev, *Complex variables bie and bem for a plane doubly periodic system of flaws*, Journal of the Chinese Institute of Engineers, 22 (1999), pp. 709–720.

[18] M. Mamode, *Fundamental solution of the Laplacian on flat tori and boundary value problems for the planar poisson equation in rectangles*, Boundary Value Problems, 2014 (2014), pp. 1–9.

[19] C. B. Moler and L. E. Payne, *Bounds for eigenvalues and eigenvectors of symmetric operators*, SIAM Journal on Numerical Analysis, 5 (1968), pp. 64–70.

[20] E. Oudet, C.-Y. Kao, and B. Osting, *Computation of free boundary minimal surfaces via extremal Steklov eigenvalue problems*, ESAIM: COCV, 27 (2021), p. 34.

[21] G. Pastras, *The Weierstrass Elliptic Function and Applications in Classical and Quantum Mechanics: A Primer for Advanced Undergraduates*, Springer, 2020.

[22] L. N. Trefethen, *Series solution of Laplace problems*, The ANZIAM Journal, 60 (2018), pp. 1–26.

[23] E. T. Whittaker and G. N. Watson, *A course of modern analysis: an introduction to the general theory of infinite processes and of analytic functions; with an account of the principal transcendental functions*, University press, 1920.

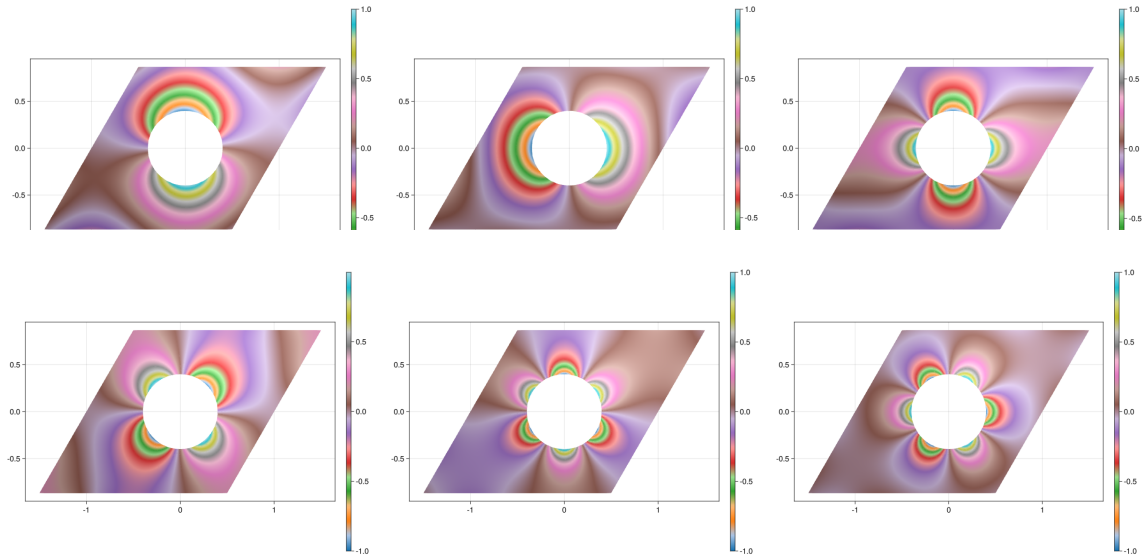

FIGURE 9. Steklov eigenfunctions of indices 2 to 7 of a punctured equilateral torus, with one hole. See section 4.3.

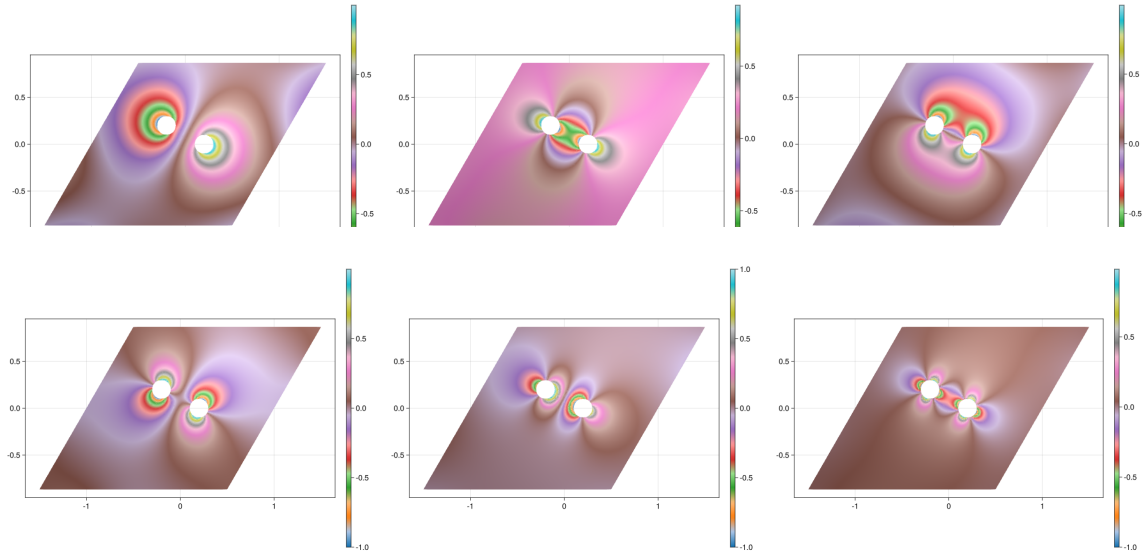

FIGURE 10. Steklov eigenfunctions of indices 2 to 7 of a punctured equilateral torus, with two holes. See section 4.3.

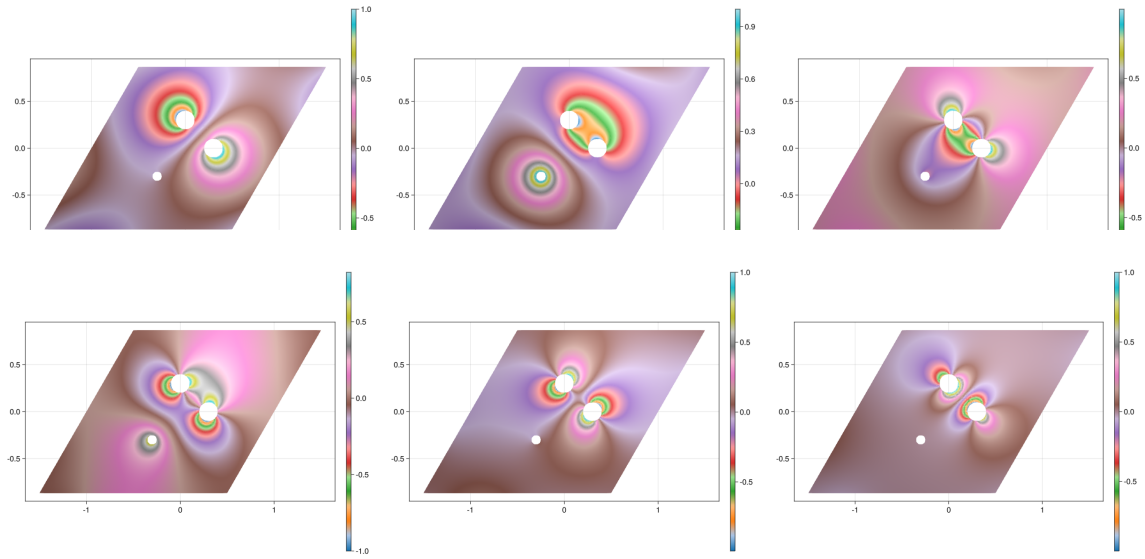

FIGURE 11. Steklov eigenfunctions of indices 2 to 7 of a punctured equilateral torus, with three holes. See section 4.3.

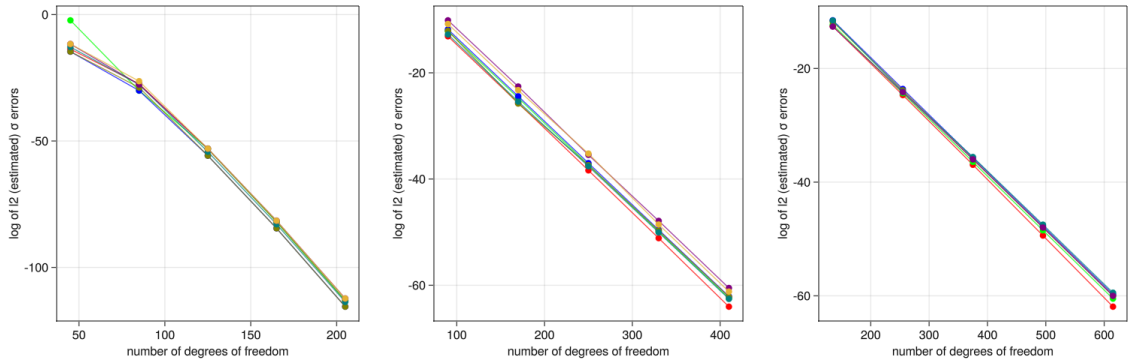

FIGURE 12. Convergence plots for Steklov eigenvalues on a square domain with 1, 2 and 3 punctured holes. Each line corresponds to one of the first seven eigenvalues. See section 4.3.

Appendix A. Computing normal derivatives

In this appendix, we provide some details for computing normal derivatives of functions of a complex variable. Denote $f(z) = u(x,y) + \imath v(x,y)$ with $z = x + \imath y$. Since f is analytic, we have $u_x = v_y$ and $u_y = -v_x$. Furthermore, $f_x = f'(z)$ and $f_y = \imath f'(z)$. Thus, with $n = n_1 + \imath n_2$, we have

$$\begin{aligned} u_n &= n_1 u_x + n_2 u_y = n_1 u_x - n_2 v_x = \Re\left[(n_1 + \imath n_2)(u_x + \imath v_x)\right] = \Re(n f'(z)) \\ v_n &= n_1 v_x + n_2 v_y = -n_1 u_y + n_2 v_y = -\Im(n_1 + \imath n_2)(u_y + \imath v_y) = \Im(n f'(z)). \end{aligned}$$

For example, $f(z) = z^k$,

$$\begin{aligned} \left(\Re\left(z^k\right)\right)_n &= k\Re(n z^{k-1}), \\ \left(\Im\left(z^k\right)\right)_n &= k\Im(n z^{k-1}). \end{aligned}$$

If $f(z) = \wp^{(k)}(z - a_j)$,

$$\begin{aligned} \left(\Re\left(\wp^{(k)}(z - a_j)\right)\right)_n &= \Re(n\wp^{(k+1)}(z - a_j)), \\ \left(\Im\left(\wp^{(k)}(z - a_j)\right)\right)_n &= \Im(n\wp^{(k+1)}(z - a_j)). \end{aligned}$$

If $f(z) = \hat{\zeta}(z - a_j)$,

$$\begin{aligned} \left(\Re\left(\hat{\zeta}\left(z - a_j\right)\right)\right)_n &= \left(\Re\left(\zeta\left(z - a_j\right)\right)\right)_n - \left(\Re\left(\gamma_2\left(z - a_j\right) + \frac{\pi}{A}\left(z - a_j\right)^*\right)\right)_n \\ &= -\Re\left(n\wp\left(z - a_j\right)\right) - \left(\left(\Re\left(\gamma_2\right) + \frac{\pi}{A}\right) n_1 - \Im\left(\gamma_2\right) n_2\right), \\ \left(\Im\left(\hat{\zeta}\left(z - a_j\right)\right)\right)_n &= \left(\Im\left(\zeta\left(z - a_j\right)\right)\right)_n - \left(\Im\left(\gamma_2\left(z - a_j\right) + \frac{\pi}{A}\left(z - a_j\right)^*\right)\right)_n \\ &= -\Im\left(n\wp\left(z - a_j\right)\right) - \left(\Im\left(\gamma_2\right) n_1 + \left(\Re\left(\gamma_2\right) - \frac{\pi}{A}\right) n_2\right), \end{aligned}$$

If $f(z) = \log\left|\hat{\sigma}\left(z - a_j\right)\right|$,

$$\begin{aligned} \left(\log\left|\hat{\sigma}\left(z - a_j\right)\right|\right)_n &= n_1\left(\log\left|\hat{\sigma}\left(z - a_j\right)\right|\right)_x + n_2\left(\log\left|\hat{\sigma}\left(z - a_j\right)\right|\right)_y \\ &= n_1\left(\Re\left(-\frac{1}{2}\gamma_2 z^2 - \frac{1}{2}\frac{\pi}{A}|z|^2\right)\right)_x + n_2\left(\Re\left(-\frac{1}{2}\gamma_2 z^2 - \frac{1}{2}\frac{\pi}{A}|z|^2\right)\right)_y \\ &\quad + n_1\left(\log\left|\sigma\left(z - a_j\right)\right|\right)_x + n_2\left(\log\left|\sigma\left(z - a_j\right)\right|\right)_y \\ &= n_1\left(\left(-\Re\left(\gamma_2\right) - \frac{\pi}{A}\right) x + \Im\left(\gamma_2\right) y\right) + n_2\left(\Im\left(\gamma_2\right) x + \left(\Re\left(\gamma_2\right) - \frac{\pi}{A}\right) y\right) \\ &\quad + n_1\left(\Re\left(\zeta\left(z - a_j\right)\right)\right) + n_2\left(-\Im\left(\zeta\left(z - a_j\right)\right)\right) \end{aligned}$$

Appendix B. Numerical values of computed Steklov eigenvalues

Values of computed Steklov eigenvalues are given in tables 1 to 6; see section 4.3 for details.

σ_2	3.2173754079055273547388028600140003676777479820848 7
σ_3	3.2173754079055273547388028600140003676777479820848 7
σ_4	4.8509953055246769789225758913043971558146193171925 9
σ_5	5.1535808494067622354977147175423476515743596941952 5
σ_6	7.5030500841676754264263508605616524388270952643055 4
σ_7	7.5030500841676754264263508605616524388270952643055 4

Table 1. Steklov eigenvalues of a square torus with one hole.

σ_2	6.4583730884228550619840098336591209199931717911998 8
σ_3	9.0403837407771358765142996538013097029295568642098 1
σ_4	9.3293139191871163580388689511474651535756609545025 7
σ_5	11.0256151261794858632162298175626283510452322045806 3
σ_6	12.6956833171972904590821248518636913084859865810398 9
σ_7	19.7288465579034874802738233951657245957254736836252 2

Table 2. Steklov eigenvalues of a square torus with two holes.

σ_2	6.5472198377502673859847608960644258680169367663824 7
σ_3	6.7929868860254394922678351810309672440853377623295 2
σ_4	9.0271536030574738600877846458747572727597923055104 2
σ_5	9.7591137601858753325468702236760113046465841686432 9
σ_6	11.1156366182651104719154974210976988330106301090199 3
σ_7	13.0806730936112510556147515295631865817762055309638 5

Table 3. Steklov eigenvalues of a square torus with three holes

σ_2	3.3486559438026053416955028824347097196258731806427 7
σ_3	3.3486559438026053416955028824347097196258731806427 7
σ_4	4.9997888154838281323414161696911319888511755241646 5
σ_5	4.9997888154838281323414161696911319888511755241646 5
σ_6	7.4439253069094730800282448573876000890114538030762 0
σ_7	7.5564971004362451848284484063187509911973273405943 3

Table 4. Steklov eigenvalues of an equilateral torus with one hole.

σ_2	6.5379480381859791879403034912575814534484263324316 3
σ_3	9.0376080333036550334299099593194299159254138984113 4
σ_4	9.3714841978105915900773713452868490256838375666772 9
σ_5	11.0290493193601778477611921698200409559484724952081 3
σ_6	12.7022269896632500128579241838244354759516306419865 4
σ_7	19.7294071856924814846188265732475554432154123443383 9

Table 5. Steklov eigenvalues of an equilateral torus with two holes.

σ_2	6.6353073708566750524643943275658007746948049885042 4
σ_3	6.9442449447168080897006161294899119295047814147480 6
σ_4	9.0231842030247917818372283778622714732126345809278 3
σ_5	9.6931125979554943330439404807456404197531403631859 0
σ_6	11.1418348194269662400678635776834974632536543564153 1
σ_7	13.0927098808612522948528106375850086733254883568756 5

Table 6. Steklov eigenvalues of an equilateral torus with three holes.